N-Element Biomimetic Antenna Arrays

Patrik Grüner, *Member, IEEE*, Ines Dorsch, and Christian Waldschmidt, *Senior Member, IEEE*

Abstract—Modern communication and sensor systems are in need of antenna front ends providing a high angular resolution. This requirement inherently leads to large and sometimes bulky antenna systems. Biomimetic antenna arrays (BMAAs), however, can provide a high angle estimation performance while occupying little space. The concept adapted from the hearing system of the fly *Ormia ochracea* has become of great interest recently. While most of the latest works focused on BMAAs with two antenna elements only, this article presents a comprehensive general theory for designing BMAAs with an arbitrary but even number of antenna elements. A scalable equivalent electrical circuit and an associated modal analysis are presented, and the effects of varying levels of biomimetic coupling are highlighted. The methodology presented in this article is applied to the design of a BMAA with four antenna elements at $76.5\,\mathrm{GHz}$ of which a prototype was fabricated and measured using radar measurements.

Index Terms—Antenna arrays, biologically inspired antennas, biomimetic antenna arrays (BMAAs), direction-of-arrival (DOA) estimation.

I. INTRODUCTION

AN INCREASING demand of modern radar sensors is the ability to measure the angle of a target relative to the sensor axis. Especially for sensors operating in multitarget scenarios, a high angular separability is required [1]–[4]. This leads to large and often bulky antenna front ends with a high number of antenna elements [5]. However, if the available space or the number of realizable antenna elements is limited, alternative solutions have to be found in order to achieve a high angular separability.

A widely used method is the application of multiple-input–multiple-output (MIMO) radars, where a comparably large virtual aperture is formed by the spatial convolution of the smaller transmitting and receiving apertures [6], [7]. Other concepts envisage the use of superresolution algorithms in the signal processing domain [8], [9].

Yet, another possibility is the application of a biomimetic antenna array (BMAA). In order to improve the angle estimation performance, this antenna system is designed to adapt a concept from nature and mimic the dynamical properties of the hearing system of the parasitoid fly *Ormia ochracea* [10], [11]. This fly is dependent on a host cricket in order to reproduce

and lay its eggs. The cricket is located by the fly via its mating call with a frequency at around $5\,\mathrm{kHz}$ [12], [13], whereby the wavelength of this mating call is significantly greater than the ear spacing of the fly. Despite this extremely small acoustical aperture, an estimation accuracy of $1°$–$2°$ is achieved by the fly due to a special mechanical coupling between its ears [10].

The BMAA concept, adapted from nature, has inspired many research groups. The mechanical coupling has been transformed into an electrical system, and different ways to model and realize the so-called biomimetic coupling (BMC) have been proposed and continually improved [11], [14]–[17]. A wide range of frequencies were considered in recent BMAA designs, including the microwave range around $400\,\mathrm{MHz}$ [18], [19] and $600\,\mathrm{MHz}$ [11], [14], as well as the lower and upper millimeter-wave (mm-wave) ranges around $20\,\mathrm{GHz}$ [20] and $77\,\mathrm{GHz}$ [15], [21], respectively. Typically, BMAAs are applied in order to increase the angular resolution of an antenna array with fixed interelement spacing. This is, e.g., useful if the wavelength of a system is large compared to the available space and the antenna elements therefore cannot provide a large spacing. However, the biomimetic principle is not limited to very small antenna spacings but can be applied to any antenna array in order to further improve their performance in terms of angular resolution [15]. Another use case of BMAAs is to reduce the space requirement of the antenna array while maintaining the angular performance. This is especially helpful if an expensive technology has to be used, as, e.g., in on-chip applications. Thus, recent applications of BMAAs are found in direction finding and localization systems [22] at comparably low frequencies as well as in compact radar systems [23]. The increased angle estimation capability of systems utilizing BMAAs was verified by means of measurements and by computing the Cramer–Rao bound (CRB) for direction-of-arrival (DOA) estimations [24]–[26].

However, almost all of the previous works on BMAAs considered arrays with two antenna elements only. This is quite obvious because the fly—as the inspiration for the antenna system—has only two ears. If the antenna front ends for high-resolution sensor systems are required, however, a considerably larger number of antenna elements are necessary. The first approaches to increase the number of antenna elements in a BMAA are found in [27] and [28] where the modeling, design, and measurement of a three-element BMAA arranged in a linear array and a triangular lattice are presented, respectively. The design process, however, is mainly based on an optimization process and is not easily scalable to an arbitrary number of antenna elements. A five-element BMAA is discussed in [29] with pairwise coupled dipole
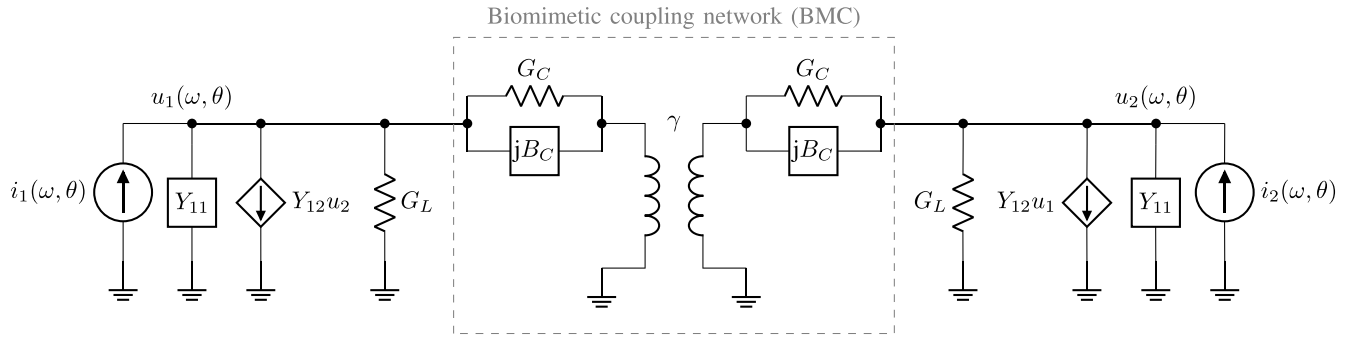
Fig. 1.   Generalized electrical model of a two-element BMAA with an external coupling network (from [15]).

antennas arranged in a linear array. However, the system is only analyzed on a high abstraction level using Monte Carlo simulations, and neither a circuit was presented nor a prototype was fabricated and measured.

This article presents a comprehensive, general concept for designing and analyzing BMAAs with an arbitrary but even number of antenna elements. The concept is thoroughly investigated theoretically, starting from the model of the two-element BMAA in [15]. A systematic extension scheme is presented, and a modal analysis of the designed circuit is outlined. Based on the investigations, an exemplary prototype of a four-element BMAA in the 77-GHz range is designed, manufactured, and measured. The measurements confirm the theoretical findings and show a phase gain of up to 2.4. This article is organized as follows. Section II introduces the basics of two-element BMAAs necessary for the extension to BMAAs with more than two elements presented in Section III. Section IV shows the practical design and measurement of a BMAA with four elements at 76.5 GHz.

II. BMAA BASICS

This section briefly summarizes the current theory of two-element BMAAs as a basis for the multichannel BMAAs and introduces terms and metrics necessary for describing BMAAs. The content of this section is described in more detail in [15].

The electrical model of a two-element BMAA [15] is shown in Fig. 1. The antenna elements are modeled by a Norton equivalent current source with short-circuit current $i_1(\omega, \theta)$ and $i_2(\omega, \theta)$—depending on the frequency $\omega/2\pi$ and the incidence angle θ—and a self-admittance Y_{11}, which is identical for both antennas sharing the same antenna design. Furthermore, the mutual coupling between the antenna elements is modeled by a voltage-controlled current source with transadmittance Y_{12}. The outputs of the system are given by the voltages $u_1(\omega, \theta)$ and $u_2(\omega, \theta)$ measured across the load conductance G_L. The BMC network consists of a transformer with a turning ratio of $\gamma = -1$, two conductances G_C, and two susceptances B_C realized as capacitor or inductor, depending on the component value.

As two antenna elements and, therefore, two input currents to the system i_1 and i_2 are considered, the circuit behavior can be fully described by the superposition of two linearly
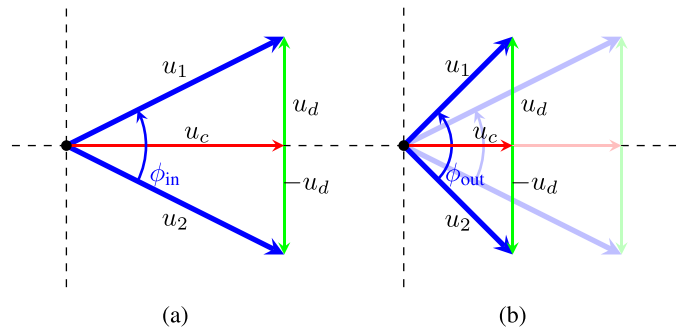

Fig. 2.   Vector plots for the generalized BMAA model at a fixed incidence angle (a) without and (b) with the BMC (from [15]).

independent exciting modes [30]. These modes are usually chosen as the common mode ($|i_1| = |i_2|$, $\arg i_1 = \arg i_2$) and the differential mode ($|i_1| = |i_2|$, $\arg i_1 = -\arg i_2$) of excitation [11], [15]. The BMC network acts as a kind of filter, which only attenuates the voltages due to the common-mode excitation and leaves the voltages due to the differential mode excitation unaltered. The attenuation depends on the component values G_C and B_C.

This working principle is summarized using the vector plots in Fig. 2. Fig. 2(a) shows the output signals u_1 and u_2 of the conventional, uncoupled antenna array for an arbitrary but fixed incidence angle $\theta \neq 0$. u_1 and u_2 exhibit identical amplitudes, and the phase difference ϕ_{in} is equal to that of the exciting signals i_1 and i_2, which follows:

$$\phi_{\text{in}}(\theta) = \arg\left(\frac{i_1(\omega, \theta)}{i_2(\omega, \theta)}\right) = 2\alpha(\theta) = kd \sin\theta \qquad (1)$$

where d is the antenna element spacing, $k = 2\pi/\lambda$ is the wavenumber in free space, λ is the wavelength of the incident wave, and $\alpha(\theta)$ is an auxiliary quantity in order to display subsequent formulas in a concise way. Fig. 2(b) shows the same situation when applying the BMC. Here, the common-mode part of the output signals is significantly attenuated, whereas the differential mode voltage is the same as in Fig. 2(a). As a consequence, the output signals u_1 and u_2 show a larger mutual phase difference ϕ_{out} at a lower signal amplitude due to the BMC.

The fundamental tradeoff of the BMAA system can be deduced from the vector plots. Every increase in phase dif-
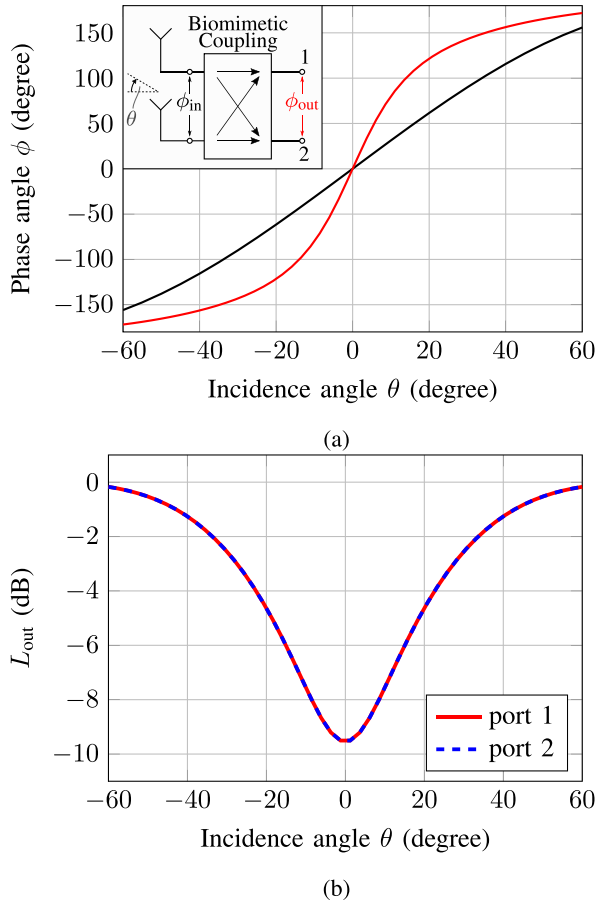
(a)

(b)

Fig. 3. BMAA with phase gain $\eta = 3$ and $L_{out} = -9.5\,dB$. (a) Typical phase progression of a conventional (———) and a biomimetic (———) antenna array. (b) Output power level L_{out}. The two curves for L_{out} are identical and lie on top of each other.

ference leads to a reduction in output level. Two parameters have been introduced in order to describe this BMAA behavior on a system level [11], [15]. The phase gain η relates the slope of the phase progression with respect to the incidence angle θ of the BMAA with that of a conventional antenna array with identical antenna elements and spacing and is defined as

$$\eta = \frac{d\phi_{out}}{d\theta}\bigg|_{\theta=0} \bigg/ \frac{d\phi_{in}}{d\theta}\bigg|_{\theta=0}. \qquad (2)$$

The second parameter is the normalized output level L_{out}, which normalizes the power at the BMAA ports to the power measured at the ports of a regular antenna array, i.e.,

$$L_{out} = \frac{P_{out,BMAA}}{P_{out,reg.\,Array}} \qquad (3)$$

and takes the values between 0 and 1.

Fig. 3 shows the typical plots of the phase progression and the normalized output power for a BMAA with $d = \lambda/2$, $\eta = 3$, and $L_{out} = -9.5\,dB$ at $\theta = 0°$.

III. DESIGN OF N-ELEMENT BMAAS

As a first step in the design of N-element BMAAs, N linearly independent exciting modes are synthesized for an array consisting of N antenna elements. In a second step, the
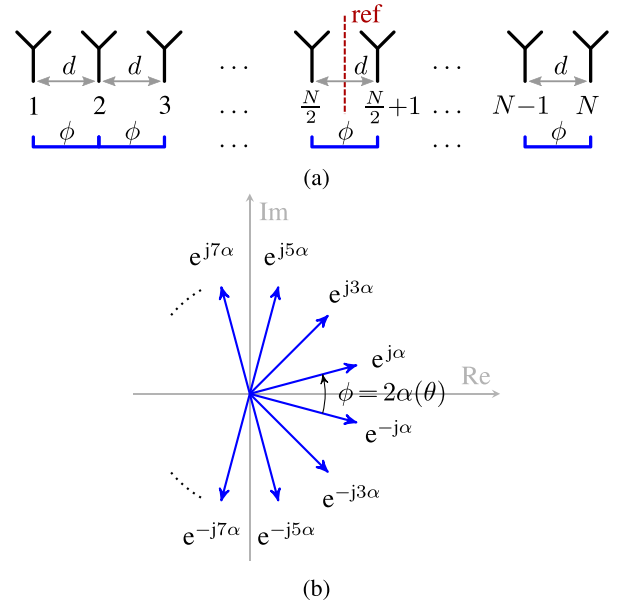

(a)

(b)

Fig. 4. (a) Antenna array consisting of N equal antenna elements spaced at a distance d and (b) antenna excitation currents $i_{1...N}(\theta) = e^{\pm jm\alpha}$ with $m = 1, 3, \ldots, N-1$ for an N-element array depicted as vectors in the complex plane for a fixed incidence angle θ. The amplitudes A_0 have been set to 1 in the figure.

circuit representation of N-element BMAAs is introduced, and a modal analysis of the BMAA, excited by the previously derived modes, is performed.

A. Excitation Through Linearly Independent Modes

If a plane wave impinges under an angle θ on an antenna array consisting of N antenna elements (N even) spaced at a distance d [see Fig. 4(a)], a total number of N complex valued currents are excited at the single antennas. Based on the definitions in Section II and by setting the reference point into the center of the array, these exciting currents $i_{1...N}(\theta)$ are given by

$$\begin{aligned} \boldsymbol{i}(\theta) &= \left(i_1(\theta), i_2(\theta), \ldots, i_{\frac{N}{2}}(\theta), i_{\frac{N}{2}+1}(\theta), \ldots, i_N(\theta)\right)^{\mathsf{T}} \\ &= A_0\left(e^{-j(N-1)\alpha}, e^{-j(N-3)\alpha}, \ldots, e^{-j\alpha}, e^{j\alpha}, \ldots, e^{j(N-1)\alpha}\right)^{\mathsf{T}} \end{aligned} \qquad (4)$$

with equal amplitudes A_0 and a mutual phase progression $\phi(\theta) = 2\alpha(\theta)$ between two adjacent antenna elements. Fig. 4(b) shows an exemplary realization of these currents in the complex plane for one incidence angle θ and $A_0 = 1$.

As it was shown in Section II, two linearly independent modes—namely the common mode and the differential mode—are sufficient to describe the exciting currents of a two-element BMAA. However, a total number of N modes have to be introduced for N antenna elements in order to synthesize all arising excitation signals by a superposition of the single modes. The N basic modes may be chosen freely as far as all arising antenna signals can be represented by a weighted superposition of these modes. Furthermore, the modes have to be linearly independent of each other. The approach chosen in this work is to separate the antenna

IEEE TRANSACTIONS ON ANTENNAS AND PROPAGATION, VOL. 69, NO. 7, JULY 2021

excitation signals $i(\theta)$ into a mode vector $i_{\mathrm{mode}}(\theta)$ and into a scaling matrix D by

$$i(\theta) = D \cdot i_{\mathrm{mode}}(\theta). \tag{5}$$

In order to obtain the mode vector and the scaling matrix, every component of the vector from (4) is rewritten by Euler's formula. As a result, an expression is yielded, which contains the m-fold angle multiples of the functions $\cos()$ and $\sin()$

$$A_0\,e^{\pm j m\alpha} = A_0(\cos(m\alpha) \pm j\sin(m\alpha)). \tag{6}$$

The m-fold angle multiples can in turn be expressed as a polynomial of degree m consisting of powers of the functions $\cos\alpha$ and $\sin\alpha$ by substituting [31]

$$\cos(m\alpha) = T_m(\cos\alpha) \tag{7}$$
$$\sin(m\alpha) = (-1)^{\frac{m-1}{2}} T_m(\sin\alpha) \tag{8}$$

into (6). $T_m(x)$ is the Chebyshev polynomial of the first kind and order m and can be calculated by the recursion formula [32]

$$T_{m+1} = 2x T_m(x) - T_{m-1}(x) \tag{9}$$

for $m \in \mathbb{N}$ and with $T_0(x) = 1$, $T_1(x) = x$.

The N independent modes $i_{\mathrm{mode},n}$ with $n = 1, 2, \ldots, N$ are chosen from the polynomials in a way that allows an extension to an arbitrary even number of antenna elements. A common mode for which all antenna elements are excited by the same signal is ensured for all realizations. The choice of the modes is performed as follows. One half of the modes (numbered 1 to $(N/2)$) are composed of powers of $\cos\alpha$ and form the real parts of the complex exciting currents. The remaining modes (numbered $(N/2) + 1$ to N) are made up of powers of $\sin\alpha$ and form the imaginary part of the exciting currents. Considering N antenna elements and setting without loss of generality $A_0 = 1$, the mode vector i_{mode} is constructed as follows:

$$
\begin{pmatrix}
i_{\mathrm{mode},1} \\
\vdots \\
i_{\mathrm{mode},k} \\
\vdots \\
i_{\mathrm{mode},\frac{N}{2}} \\
i_{\mathrm{mode},\frac{N}{2}+1} \\
\vdots \\
i_{\mathrm{mode},l} \\
\vdots \\
i_{\mathrm{mode},N}
\end{pmatrix}
=
\begin{pmatrix}
\cos^{N-3}\alpha - \cos^{N-1}\alpha \\
\vdots \\
\cos^{N-(2k+1)}\alpha - \cos^{N-(2k-1)}\alpha \\
\vdots \\
\cos^{N-1}\alpha \\
\sin^{N-1}\alpha \\
\vdots \\
\sin^{-N+2l-3}\alpha - \sin^{-N+2l-1}\alpha \\
\vdots \\
\sin^{N-3}\alpha - \sin^{N-1}\alpha
\end{pmatrix}
\tag{10}
$$

with $k = 1, 2, \ldots, (N/2) - 1$ and $l = (N/2) + 2, (N/2) + 3, \ldots, N$.

The scaling matrix D is a square matrix of dimension $N \times N$ and is directly deduced from the Chebyshev polynomials. Considering the polynomial of the exciting current $e^{\pm j m\alpha}$ with m-fold multiple of α and $m = 1, 3, \ldots, N - 1$, the prefactor of $\cos^i\alpha$ is named $a_{i,m}$ and the prefactor of $\sin^i\alpha$ is named $b_{i,m}$. If the mode vector i_{mode} is chosen according to (10), then the scaling matrix D expands from the center to the outside

according to Fig. 5, starting from the two-element case with the scaling matrix

$$D_0 = \begin{pmatrix} 1 & -j \\ 1 & j \end{pmatrix}. \tag{11}$$

The submatrices for four, six, and eight antennas are marked in Fig. 5 accordingly.

Inserting the constructed scaling matrix into (5), it can be noted that mode $(N/2)$ is scaled equally for all antennas. Thus, this mode represents the desired common mode. Modes $1, \ldots, (N/2)$ are real and symmetrical regarding its column center and represent the even modes. In contrast, modes $(N/2) + 1, \ldots, N$ are purely imaginary and are mirror-symmetrical with opposite signs with respect to their column centers. Modes $(N/2) + 1, \ldots, N$ represent the odd modes, whereas mode $(N/2) + 2$ is closest to the classical differential mode.

As an example, the modal representation according to (5) for the first $(i_1(\theta))$ and the last $(i_6(\theta))$ antenna excitation signal for $N = 6$ is given

$$
e^{\pm j5\alpha} = \underbrace{5}_{a_{1,5}}\cos\alpha \underbrace{-20}_{a_{3,5}}\cos^3\alpha \underbrace{+16}_{a_{5,5}}\cos^5\alpha
$$
$$
\pm j(\underbrace{5}_{b_{1,5}}\sin\alpha \underbrace{-20}_{b_{3,5}}\sin^3\alpha \underbrace{+16}_{b_{5,5}}\sin^5\alpha) \tag{12}
$$
$$
= -15\underbrace{(\cos^3\alpha - \cos^5\alpha)}_{i_{\mathrm{mode},1}} + 5\underbrace{(\cos\alpha - \cos^3\alpha)}_{i_{\mathrm{mode},2}} + \underbrace{\cos^5\alpha}_{i_{\mathrm{mode},3}}
$$
$$
\mp j(\underbrace{\sin^5\alpha}_{i_{\mathrm{mode},4}} + 5\underbrace{(\sin\alpha - \sin^3\alpha)}_{i_{\mathrm{mode},5}} - 15\underbrace{(\sin^3\alpha - \sin^5\alpha)}_{i_{\mathrm{mode},6}}).
$$
$$\tag{13}$$

The presented method for the construction of N linearly independent exciting modes is a universal approach not being limited to BMAAs. It also covers the common-/differential-mode excitation of two-element BMAAs used in recent works [11], [15].

B. Assembly of the N-Element BMAA Circuit

This section discusses how the BMAA circuit in Fig. 1 is extended to the N-antenna case. The choice of which antennas are to be biomimetically coupled for $N > 2$, however, leaves room for variations. For the sake of straightforward realizability on planar printed circuit boards (PCBs) without the need of transitions to other metal layers, only a BMC of neighboring antenna elements is considered in this work.

The assembly of N biomimetically coupled antennas is carried out by means of two different functional blocks, as shown in Fig. 6. The first block, which is marked by a dashed frame in Fig. 6, represents the antenna. This block is analogical to the circuitry representing the antenna in Fig. 1 with $Y_{\mathrm{S},n}$ being the parallel connection of the antenna self-admittance Y_{nn} and the load conductance G_{L}.

The second functional block, marked by a dotted frame in Fig. 6, represents the BMC network. It consists, similar to Section II, of a transformer with a coupling ratio of $\gamma = -1$ and a coupling admittance Y_{C}. The coupling admittance Y_{C}

$$
D =
\begin{pmatrix}
\ddots & \vdots & \vdots & \vdots & \vdots\;\vdots & \vdots & \vdots & \vdots & \iddots \\
\cdots & (a_{1,7}+a_{3,7}+a_{5,7}) & (a_{1,7}+a_{3,7}) & a_{1,7} & 1\;\;\;\mathrm{j} & -\mathrm{j}b_{1,7} & -\mathrm{j}(b_{1,7}+b_{3,7}) & -\mathrm{j}(b_{1,7}+b_{3,7}+b_{5,7}) & \cdots \\
\cdots & 1 & (a_{1,5}+a_{3,5}) & a_{1,5} & 1\;\;\;-\mathrm{j} & -\mathrm{j}b_{1,5} & -\mathrm{j}(b_{1,5}+b_{3,5}) & -\mathrm{j} & \cdots \\
\cdots & 1 & 1 & a_{1,3} & 1\;\;\;\mathrm{j} & -\mathrm{j}b_{1,3} & \mathrm{j} & \mathrm{j} & \cdots \\
\cdots & 1 & 1 & 1 & 1\;\;\;-\mathrm{j} & -\mathrm{j} & -\mathrm{j} & -\mathrm{j} & \cdots \\
\cdots & 1 & 1 & 1 & 1\;\;\;\mathrm{j} & \mathrm{j} & \mathrm{j} & \mathrm{j} & \cdots \\
\cdots & 1 & 1 & a_{1,3} & 1\;\;\;-\mathrm{j} & \mathrm{j}b_{1,3} & -\mathrm{j} & -\mathrm{j} & \cdots \\
\cdots & 1 & (a_{1,5}+a_{3,5}) & a_{1,5} & 1\;\;\;\mathrm{j} & \mathrm{j}b_{1,5} & \mathrm{j}(b_{1,5}+b_{3,5}) & \mathrm{j} & \cdots \\
\cdots & (a_{1,7}+a_{3,7}+a_{5,7}) & (a_{1,7}+a_{3,7}) & a_{1,7} & 1\;\;\;-\mathrm{j} & \mathrm{j}b_{1,7} & \mathrm{j}(b_{1,7}+b_{3,7}) & \mathrm{j}(b_{1,7}+b_{3,7}+b_{5,7}) & \cdots \\
\iddots & \vdots & \vdots & \vdots & \vdots\;\vdots & \vdots & \vdots & \vdots & \ddots
\end{pmatrix}
$$

8 antennas · 6 antennas · 4 antennas · D_0

mode no. $\quad\frac{N}{2}-3\qquad\frac{N}{2}-2\qquad\frac{N}{2}-1\;\;\frac{N}{2}\;\;\frac{N}{2}+1\;\;\frac{N}{2}+2\qquad\frac{N}{2}+3\qquad\qquad\frac{N}{2}+4$

Fig. 5. Construction principle of the scaling matrix D for an increasing number of antennas N, starting with the matrix D_0 for the case of two antennas. Each column n represents the scaling factors associated with mode n.

Fig. 6. Equivalent circuit representation of an antenna (left box) and the BMC network (right box) as building blocks of a BMAA with an arbitrary number of antenna elements.

can hereby be regarded as a parallel connection of a conductance G_C and a susceptance B_C. The coupling admittance can be found symmetrically on both sides of the transformer. Depending on the desired order N of the BMAA, the circuit consequently consists of N antenna blocks and $N-1$ blocks representing the BMC, lying in between two antenna blocks.

C. Modal Analysis of the N-Element BMAA Circuit

The aim of the modal analysis is to calculate the voltages $u_n(\omega,\theta)$ in Fig. 6 depending on the excitation and the component values in the BMAA circuit. In order to analyze the circuit synthesized with the functional blocks of Fig. 6, it is excited by the N modes defined in Section III-A. The short-circuit current i_n of the current source modeling the nth antenna always corresponds to a mode definition where the weighted superposition of the N modes yields the complex-valued signal $\mathrm{e}^{\pm \mathrm{j}m\alpha}$

$$i_n(\omega,\theta) = \mathrm{e}^{\pm \mathrm{j}m\alpha} = \sum_{m=1}^{N} D_{n,m} i_{\mathrm{mode},m}. \tag{14}$$

In order to perform the calculations, some assumptions are made. All antenna elements are considered equal, i.e., the radiating elements are assumed identical, and no edge effects are considered. The mutual coupling between the antenna elements is neglected. This assumption is valid as long as the mutual coupling is small compared to the BMC through the transformer [15]. Another prerequisite resulting from Section III-A is an even number N of antenna elements. Furthermore, it is assumed that the component values of the BMC are chosen symmetrically across the array, i.e., $Y_{\mathrm{C},i} = Y_{\mathrm{C},N-i}$ with $i = 1, 2, \ldots, (N/2)$.

The modal analysis in its general form has to be performed individually depending on the specified number N of antenna elements. However, some characteristics and simplifications, which are generally applicable, are highlighted in the remainder of this section. A detailed analysis of a BMAA with four antenna elements is presented afterward in Section IV.

1) Even Modes: Modes 1 to $(N/2)$ are composed of even functions. Accordingly, the antenna array is excited symmetrically with respect to its point of symmetry (see the dashed line in Fig. 7). The magnitude of the currents $i_{x,l}$ and $i_{x,r}$ in Fig. 7 is identical due to the symmetrical excitation on both sides of the array and point toward the transformer ($i_{x,r} < 0$). The voltage u_l on the left side of the transformer is consequently identical to the voltage u_r on the right side of the transformer. By transforming with a turning ratio of $\gamma = -1$, these voltages are inverted (u_r', u_l') and cancel each other on either side of the transformer. The potentials $u_{x,l}$ and $u_{x,r}$, therefore, represent a virtual ground, and thus, the whole BMAA is divided into two identical parts. The currents $i_{x,l}$ and $i_{x,r}$ flowing through the coupling admittances Y_C on either side of the transformer are identical but not zero and
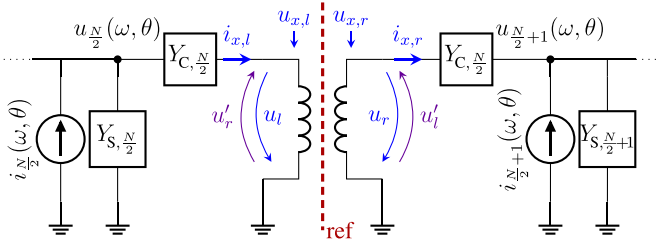
Fig. 7. Cutout of the equivalent circuit of an N-element BMAA around the array center (red dashed) with currents and voltages for the modal analysis.

Fig. 8. Equivalent circuit representation of an N-element BMAA when excited with an odd excitation mode.

therefore lead to a parallel connection of Y_C with $Y_{S,(N/2)}$ and $Y_{S,(N/2)+1}$, respectively. Because of these admittances connected in parallel and because the weighting factors of the modes are not equal for all antenna elements, the remaining circuits are not symmetrical anymore with respect to their new center point. Thus, the voltages $u_n(\omega, \theta)$ have to be calculated individually depending on the number of antenna elements. However, for all even modes, only one half of the BMAA has to be considered.

2) Odd Modes: Mode $(N/2) + 1$ is a purely imaginary mode where all antennas are excited with identical magnitude but with an alternating sign and therefore represents an odd mode. As a consequence, every two neighboring current sources in the electrical model are now directed in opposite directions.

In order to analyze the circuit excited with this mode, the simplified schematic in Fig. 8 is considered. The left and the right side with respect to the middle transformer are combined into one block consisting of a current source and a load admittance. The current sources are directed oppositely due to the odd excitation. Due to the assumption of equal antenna elements and symmetrical component values in the BMC, the current sources are loaded by the same load admittance Y_{load}. When transforming the current $i_{A,l}$ in Fig. 8 which is formed by a current divider between load and BMC across the transformer with turning ratio $\gamma = -1$, it can be seen that the currents $i_{A,l}$ and $i_{A,r}$ are directed in opposite directions and, therefore, cancel each other. As a result, no current is flowing through the coupling admittance $Y_{C,(N/2)}$ and the whole coupling network can be replaced by an open circuit $(Y_{C,(N/2)} = 0\,\mathrm{S})$.

The same procedure can now be repeated for the remaining halves of the electrical circuit. It is obvious that each remaining circuit can again be represented by an equivalent circuit as in Fig. 8. Every coupling network can therefore be replaced by an open circuit $(Y_C = 0\,\mathrm{S})$, and consequently, all antenna elements in the array are decoupled from each other when the array is excited with mode $(N/2) + 1$. It should be noted that this mode is included in every BMAA design, regardless of the number of antenna elements.

Modes $(N/2) + 2$ up to N are also purely imaginary, odd modes, but the antenna currents are not equal in amplitude, in contrast to the aforementioned mode $(N/2) + 1$. The outer antennas in the array are given higher weighting than
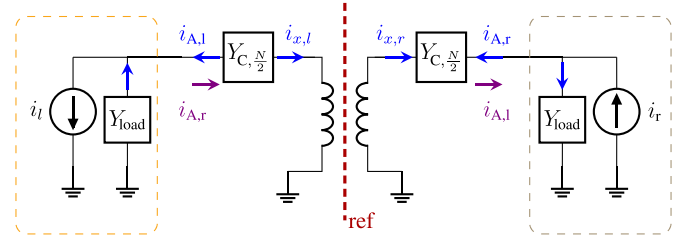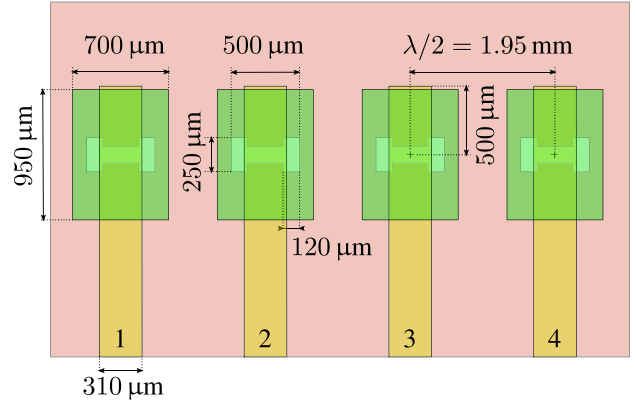
Fig. 9. Top view of the four-antenna array consisting of aperture coupled patches. The patches are on the top metal layer (green, L1), whereas the microstrip lines (yellow, L4) lie on the bottom layer. The ground plane (red, L3) carrying the coupling slots is located in between the top and bottom layers.

the antennas on the inside of the array. Due to the odd excitation and the assumed equality of the self-admittances of the antennas, the currents through the coupling network in the symmetry plane cancel each other, and the coupling network can be replaced by an open circuit, like it was shown before for mode $(N/2) + 1$. However, the resulting circuit halves are, in contrast to mode $(N/2) + 1$, not excited by current sources with identical amplitudes. Therefore, no further simplification can be applied and an analysis depending on the actual number of antenna elements has to be performed.

IV. REALIZATION OF A FOUR-ELEMENT BMAA

This section describes the realization of a BMAA with four antenna elements (4-BMAA) at a frequency of 76.5 GHz. After choosing suitable antenna elements, the design process and analysis based on the theory derived in Section III are presented. A fabricated prototype is measured using radar measurements.

A. Antenna Elements and Circuit Representation

The planar, aperture-coupled patch antenna array used in this work is based on the antenna array in [15] and is shown in Fig. 9. The stack-up consists of four metal and two RO3003 substrate layers with 127 μm height, laminated by RO3001. The microstrip lines are placed on the bottom metal layer (L4) with the coupling slots located above in the ground metal layer L3. The metal layer L2 is removed to not alter the feeding
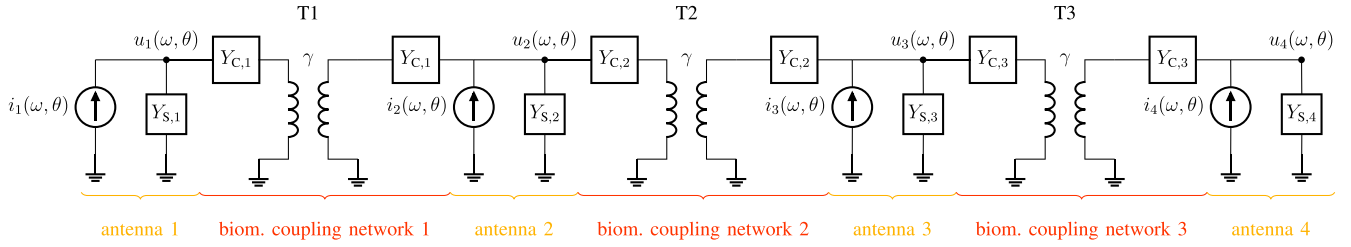
Fig. 10. Equivalent electrical circuit of a four-element BMAA consisting of four antennas and three BMC networks.

TABLE I
Y-PARAMETER OF THE FOUR-ANTENNA ARRAY OF FIG. 9 AT 76.5 GHz EXTRACTED FROM FULL-WAVE SIMULATIONS

	Re()	Im()		Re()	Im()
Y_{11}	17.72 mS	0.24 mS	Y_{23}	3.27 mS	4.83 mS
Y_{12}	2.94 mS	4.96 mS	Y_{24}	−1.25 mS	−1.66 mS
Y_{13}	−1.23 mS	−1.67 mS	Y_{33}	16.76 mS	0.59 mS
Y_{14}	0.47 mS	0.44 mS	Y_{34}	2.93 mS	5.00 mS
Y_{22}	16.59 mS	0.60 mS	Y_{44}	17.72 mS	0.15 mS
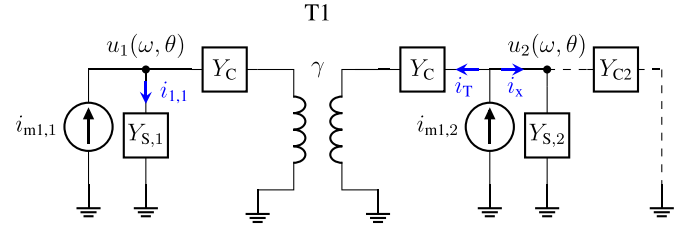
Fig. 11. Left half of the 4-BMAA circuit when excited with mode 1.

of the patch antennas located on the top metal layer (L1). The four antenna elements are arranged in a uniform linear array (ULA) and are spaced at a distance of 1.95 mm, which corresponds to half a wavelength λ in free space at 76.5 GHz. The comparably large spacing leads to a low mutual coupling between the antenna elements.

The antenna array was simulated by means of full-wave simulations, and the simulated Y-parameters at 76.5 GHz are listed in Table I. The Y-matrix is symmetrical, and because of the symmetrical arrangement of the antennas, it holds

$$Y_{11} = Y_{44} \quad Y_{12} = Y_{34}$$
$$Y_{22} = Y_{33} \quad Y_{13} = Y_{24}.$$

Furthermore, the approximation $Y_{11} = Y_{44} \approx Y_{22} = Y_{33}$ can be made. The cross admittances Y_{ij} with $i \neq j$ are in their real parts always at least one order of magnitude smaller than the self-admittances Y_{ii}. In order to reduce the complexity of the problem, these are neglected in the following considerations.

The equivalent electrical circuit diagram of the 4-BMAA is constructed according to the design specification in Fig. 6. The complete electrical circuit consisting of four antennas and three BMCs is shown in Fig. 10. Based on the assumptions made previously, the outer BMCs are chosen equally, i.e., $Y_{C,1} = Y_{C,3} = Y_C$ and different to the middle one $Y_{C,2} = Y_{C2}$.

B. Excitation and Modal Analysis

In the case of four antenna elements, there are four complex antenna signals $i_{1..4}(\omega, \theta)$, which are shown as vectors in the complex plane as a part of Fig. 4(b). Amplitude differences between the individual currents can be neglected, which is why the amplitude A_0 is set to $A_0 = 1$ without loss of generality.

In order to perform a modal analysis, the antenna signals are decomposed into exciting modes according to Section III-A.

In matrix notation, the decomposition is given as

$$\begin{pmatrix} e^{-j3\alpha} \\ e^{-j\alpha} \\ e^{j\alpha} \\ e^{j3\alpha} \end{pmatrix} = \underbrace{\begin{pmatrix} -3 & 1 & j & -3j \\ 1 & 1 & -j & -j \\ 1 & 1 & j & j \\ -3 & 1 & -j & 3j \end{pmatrix}}_{D} \begin{pmatrix} \cos\alpha - \cos^3\alpha \\ \cos^3\alpha \\ \sin^3\alpha \\ \sin\alpha - \sin^3\alpha \end{pmatrix}, \quad (15)$$

where the vector of exciting modes is constructed according to (10) with $N = 4$ and the scaling matrix D is taken from Fig. 5 for the case of four antennas.

In the following, the electrical circuit of Fig. 10 is evaluated by a modal analysis. Every exciting mode is considered separately in order to obtain an expression for the output voltages $u_n(\omega, \theta)$ with $n = 1, \ldots, 4$. These are calculated by superimposing the individual mode voltages $u_{mk,n}$ that are generated at antenna n due to the excitation with mode k

$$u_n(\omega, \theta) = \sum_{k=1}^{4} u_{mk,n}(\omega, \theta). \quad (16)$$

1) Mode 1: Mode 1 is dependent on $(\cos\alpha - \cos^3\alpha)$ and represents an even function. Thus, the array is excited symmetrically with regard to the reference plane. According to Section III-C, the center transformer can be replaced by a short circuit and only one half of the circuit has to be considered (see Fig. 11). The circuit is not symmetric anymore due to the additional admittance Y_{C2} of the central coupling network and the differently weighted antenna currents.

For further analysis, the circuit of Fig. 11 is considered separately for each of the two excitations, whereas the other current source is temporarily replaced by an open circuit. The resulting output voltages $u_{1,ant1}$ and $u_{1,ant2}$ can afterward be superimposed to get the voltage $u_{m1,1}$. In order to better illustrate the representation of parallel circuits, the algebraic equations are expressed as a function of impedances in the remainder of this section. However, the indices remain the

same as for the respective admittances, i.e., $Z_{C2} = (1/Y_{C2})$, $Z_{S,1} = (1/Y_{S,1})$, and so on. The dependence of ω and θ is omitted in the equations for reasons of compactness.

If only the excitation $i_{m1,1}(\omega, \theta)$ of antenna 1 with mode 1 is considered and the second current source is replaced by an open circuit, a passive circuit results on the right side of transformer T1. These admittances or impedances can be transformed over T1 with turning ratio $\gamma = -1$ by a ratio of $\gamma^2 = 1$ [33], i.e., the transformer can be regarded as a short circuit. However, for currents and voltages, the factor $\gamma = -1$ has to be considered, leading to a change in signs between the left and right sides of the transformer. Thus, for an excitation of only antenna 1 with $i_{m1,1}(\omega, \theta)$, the intermediate voltage $u_{m1,1,ant1}$ calculates to

$$u_{m1,1,ant1} = (((Z_{C2} \parallel Z_{S,2}) + 2Z_C) \parallel Z_{S,1})i_{m1,1}. \quad (17)$$

For an excitation of only antenna 2 with $i_{m1,2}(\omega, \theta)$, it holds for the second intermediate voltage $u_{m1,1,ant2}$

$$u_{m1,1,ant2} = Z_{S,1} i_{1,1} = Z_{S,1}(-i_T) \quad (18)$$

$$= Z_{S,1}\left(-\frac{(Z_{S,1} + 2Z_C) \parallel Z_{S,2} \parallel Z_{C2}}{2Z_C + Z_{S,1}}i_{m1,2}\right). \quad (19)$$

Equation (19) results from the current divider that splits $i_{m1,2}$ into i_T and i_x.

By superimposing (17) and (19), an equation is yielded dependent on the mode definition $i_{m1,n}$ and all occurring coupling, antenna, and load impedances. With the same approach the voltages $u_{m1,2}(\omega, \theta)$ at antenna 2, $u_{m1,3}(\omega, \theta)$ at antenna 3, and $u_{m1,4}(\omega, \theta)$ at antenna 4 can be calculated. The respective voltages are

$$u_{m1,1} = (((Z_{C2} \parallel Z_{S,2}) + 2Z_C) \parallel Z_{S,1})i_{m1,1}$$
$$-\left(\frac{(Z_{S,1} + 2Z_C) \parallel Z_{S,2} \parallel Z_{C2}}{2Z_C + Z_{S,1}}\right)Z_{S,1} i_{m1,2} \quad (20)$$

$$u_{m1,2} = (Z_{S,2} \parallel Z_{C2} \parallel (2Z_C + Z_{S,1}))i_{m1,2}$$
$$-\left(\frac{Z_{S,1} \parallel (2Z_C + (Z_{S,2} \parallel Z_{C2}))}{2Z_C + (Z_{S,2} \parallel Z_{C2})}\right)$$
$$\times (Z_{S,2} \parallel Z_{C2})i_{m1,1} \quad (21)$$

$$u_{m1,3} = (Z_{S,3} \parallel Z_{C2} \parallel (2Z_C + Z_{S,4}))i_{m1,3}$$
$$-\left(\frac{Z_{S,4} \parallel (2Z_C + (Z_{S,3} \parallel Z_{C2}))}{2Z_C + (Z_{S,3} \parallel Z_{C2})}\right)$$
$$\times (Z_{S,3} \parallel Z_{C2})i_{m1,4} \quad (22)$$

$$u_{m1,4} = (((Z_{C2} \parallel Z_{S,3}) + 2Z_C) \parallel Z_{S,4})i_{m1,4}$$
$$-\left(\frac{(Z_{S,4} + 2Z_C) \parallel Z_{S,3} \parallel Z_{C2}}{2Z_C + Z_{S,4}}\right)Z_{S,4} i_{m1,3}. \quad (23)$$

With the exception of the currents, the expressions of $u_{m1,1}(\omega, \theta)$ and $u_{m1,4}(\omega, \theta)$ are identical for the assumptions $Y_{S,1} = Y_{S,4}$ and $Y_{S,2} = Y_{S,3}$ mentioned in Section IV-A. Similarly, $u_{m1,2}(\omega, \theta)$ and $u_{m1,3}(\omega, \theta)$ are identical due to the symmetry of the array. Because of mode 1 being an even mode and $i_{m1,1}(\omega, \theta) = i_{m1,4}(\omega, \theta)$ as well as $i_{m1,2}(\omega, \theta) = i_{m1,3}(\omega, \theta)$, the voltages at antennas 1 and 4 as well as at antennas 2 and 3 are identical in pairs, respectively.

2) Mode 2: Mode 2 corresponds to a common-mode excitation of all antennas. The excitation currents of this mode are identical, i.e., $i_{m2,1} = i_{m2,2} = i_{m2,3} = i_{m2,4} = \cos^3 \alpha$. Like mode 1, mode 2 is an even function, which results in a virtual ground in the center of symmetry of the array, and the array is split into two identical halves. Thus, (20)–(23) are also valid for this mode when adjusting all currents to $i_{m2,1}$, $i_{m2,2}$, $i_{m2,3}$, and $i_{m2,4}$.

3) Mode 3: Mode 3 is a purely imaginary odd mode where all antennas are excited by the same magnitude but with alternating signs. As it was shown in Section III-C, all BMC networks can be replaced by an open circuit if assuming $Y_{S,1} = Y_{S,4} \approx Y_{S,2} = Y_{S,3}$. Thus, the individual antenna elements are completely decoupled when the array is excited by this mode. The voltages at the antennas are therefore given by

$$u_{m3,1} = Z_{S,1} i_{m3,1} \quad (24)$$
$$u_{m3,2} = Z_{S,2} i_{m3,2} \quad (25)$$
$$u_{m3,3} = Z_{S,3} i_{m3,3} \quad (26)$$
$$u_{m3,4} = Z_{S,4} i_{m3,4}. \quad (27)$$

4) Mode 4: Mode 4 is like mode 3 a purely imaginary odd mode. The antenna currents are, however, not equal in amplitude, in contrast to mode 3. As it was shown in Section III, the central transformer (in this case T2) can be replaced by an open circuit for every odd mode and the assumptions $Y_{S,1} = Y_{S,4}$ and $Y_{S,2} = Y_{S,3}$.

In contrast to mode 3, the remaining circuit halves containing T1 and T3 have to be considered in more detail because the current sources have different amplitudes. An analysis can be carried out in the same way as for mode 1 by exciting the circuit separately with each of the two current sources and superimposing the resulting voltages afterward. While the coupling admittance Y_{C2} was present in the circuit for modes 1 and 2, it is absent for mode 4. Consequently, a circuit remains as in Fig. 11 without the dashed line connecting Y_{C2}. Using this equivalent circuit, the antenna voltages of the array when excited by mode 4 calculate to

$$u_{m4,1} = ((Z_{S,2} + 2Z_C) \parallel Z_{S,1})i_{m4,1}$$
$$-\left(\frac{(Z_{S,1} + 2Z_C) \parallel Z_{S,2}}{2Z_C + Z_{S,1}}\right)Z_{S,1} i_{m4,2} \quad (28)$$

$$u_{m4,2} = (Z_{S,2} \parallel (2Z_C + Z_{S,1}))i_{m4,2}$$
$$-\left(\frac{Z_{S,1} \parallel (2Z_C + Z_{S,2})}{2Z_C + Z_{S,2}}\right)Z_{S,2} i_{m4,1} \quad (29)$$

$$u_{m4,3} = (Z_{S,3} \parallel (2Z_C + Z_{S,4}))i_{m4,3}$$
$$-\left(\frac{Z_{S,4} \parallel (2Z_C + Z_{S,3})}{2Z_C + Z_{S,3}}\right)Z_{S,3} i_{m4,4} \quad (30)$$

$$u_{m4,4} = ((Z_{S,3} + 2Z_C) \parallel Z_{S,4})i_{m4,4}$$
$$-\left(\frac{(Z_{S,4} + 2Z_C) \parallel Z_{S,3}}{2Z_C + Z_{S,4}}\right)Z_{S,4} i_{m4,3}. \quad (31)$$

C. System Evaluation

In Section IV-B, a method was presented to analyze the behavior of a BMAA with four antenna elements. By applying the derived formulas on a sample configuration of a 4-BMAA, the effects on the phase progression, the normalized output
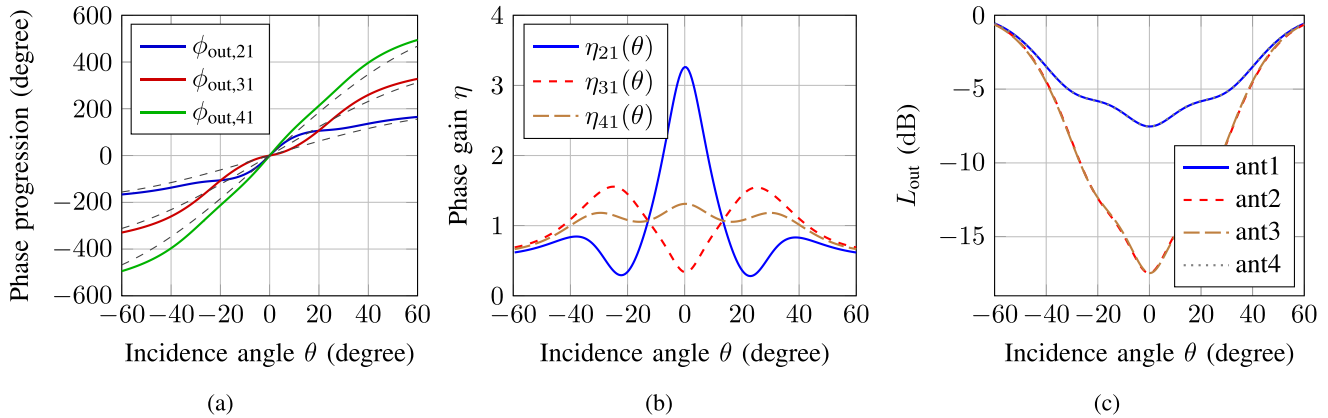
Fig. 12.   Calculated (a) phase progression, (b) phase gain, and (c) normalized output power L_{out} for a 4-BMAA with coupling network parameter $R_{\text{C}} = R_{\text{C2}} = 13\,\Omega$.

power L_{out}, and the phase gain η are highlighted in this section. The degrees of freedom in designing the 4-BMAA are the choices of the coupling admittances Y_{C} and Y_{C2}. These can, in general, be real or complex values, and they can be chosen with equal or different component values at the individual coupling networks, respectively. In the following example, all BMC admittances are considered equal with an exemplary value of $Y_{\text{C}} = Y_{\text{C2}} = 1/13\,\Omega$. The load admittance is chosen to $G_{\text{L}} = 20\,\text{mS}$ (equals $1/50\,\Omega$) and forms the admittance $Y_{\text{S,n}} = 1/Z_{\text{S,n}}$ together with the antenna self-admittance Y_{nn}.

The phase progressions between the antennas of the 4-BMAA are of special interest, together with the normalized output power L_{out}. These quantities are shown in Fig. 12(a) and (c), respectively. The phase progression ϕ_{out} is hereby normalized to the first antenna in the array. Thus, $\phi_{\text{out},21}$ denotes the phase progression between antennas 2 and 1. In general, it holds

$$\phi_{\text{out},ij}(\theta) = \arg u_i(\theta) - \arg u_j(\theta), \qquad (32)$$

where u_i and u_j are the voltages at antennas i and j calculated by the modal analysis of Section III-C. The reference antenna to compare the 4-BMAA against is a four-element ULA with the identical antenna elements and spacings but without the BMC network. The phase progressions of this ULA are shown in dashed line in Fig. 12(a) and consist of multiples of $2\alpha = kd \sin\theta$. In order to visualize the change in steepness of the phase progression of the BMAA, the angle-dependent phase gain $\eta_{ij}(\theta)$ is introduced

$$\eta_{ij}(\theta) = \frac{d\phi_{\text{out},ij}}{d\theta} \Big/ \frac{d\phi_{\text{out,conv},ij}}{d\theta}. \qquad (33)$$

This generalized phase gain that normalizes the steepness of the 4-BMAA phase progression by the steepness of the ULA phase progression is shown in Fig. 12(b). It is apparent that the phase progression $\phi_{\text{out},21}$ between the first two antennas has its maximum slope in the main radiation direction $\theta = 0°$. Consequently, the phase gain reaches its maximum also at this angle with a value of $\eta_{21}(\theta = 0°) = \eta_{21} = 3.3$. In

TABLE II
4-BMAA PARAMETERS WHEN VARYING THE REAL COUPLING
RESISTANCE $R_{\text{C}} = R_{\text{C2}}$

$R_{\text{C}} = R_{\text{C2}}$	$\max(\eta_{21}(\theta))$	$\max(\eta_{31}(\theta))$	$\max(\eta_{41}(\theta))$
$2\,\Omega$	40	$5.6\ @\ \theta = \pm28°$	3.1
$5\,\Omega$	12	$2.8\ @\ \theta = \pm27°$	1.8
$10\,\Omega$	4.4	$1.8\ @\ \theta = \pm25°$	1.4
$20\,\Omega$	2.2	$1.3\ @\ \theta = \pm25°$	1.2
$40\,\Omega$	1.4	$1.1\ @\ \theta = \pm24°$	1.1

$R_{\text{C}} = R_{\text{C2}}$	$\min(L_{\text{out},1/4})$	$\min(L_{\text{out},2/3})$
$2\,\Omega$	$-18\,\text{dB}$	$-42\,\text{dB}$
$5\,\Omega$	$-12\,\text{dB}$	$-29\,\text{dB}$
$10\,\Omega$	$-9\,\text{dB}$	$-20\,\text{dB}$
$20\,\Omega$	$-6\,\text{dB}$	$-13\,\text{dB}$
$40\,\Omega$	$-3.8\,\text{dB}$	$-8\,\text{dB}$

contrast, the phase progression $\phi_{\text{out},31}$ is flatter around the main radiation direction than the classically expected $2kd \sin\theta$ curve of the ULA, which is why $\eta_{31}(\theta)$ is smaller than one in an angular range of $\theta = \pm12°$. The advantage of $\phi_{\text{out},31}$, however, is a phase gain of around 1.7 with respect to the ULA at the incidence angles $\theta = \pm25°$. The phase progression $\phi_{\text{out},41}$ between the two outer antennas is steeper than $3kd \sin\theta$ for the whole angular range $\theta = -40°\ldots40°$. However, the phase gain $\eta_{41}(\theta)$ is only marginally above one.

The BMC is accompanied by a loss in output power, which can be seen in Fig. 12(c). However, the output power does not decrease in the same way at all antennas, but all antennas show most of its power loss in the main beam direction $\theta = 0°$. Outer antennas 1 and 4 experience the same attenuation of up to 7.5 dB and internal antennas 2 and 3 also experience the same attenuation of up to 17.5 dB. Just like the phase gains from Fig. 12(b), the output power in Fig. 12(c) shows a ripple.

An increase of the real coupling resistance $R_{\text{C}} = R_{\text{C2}}$ leads to a decrease of the phase gain, while the overall shape of the curves remains the same. Consequently, L_{out} increases. Table II shows the 4-BMAA parameters considered above for different values of the coupling resistance. Especially, the configuration with $R_{\text{C}} = 2\,\Omega$ has to be considered as a theoretical extreme value.

If the antenna array under consideration is supposed to be implemented in a direction finding system or an imaging radar, a good measure to evaluate its performance is the array ambiguity function (AF) [34]. It is used to estimate the ambiguities resulting from an angle estimation using the specific array. The evaluation of the array AF is done with the help of the antenna steering vector $\boldsymbol{a}(\theta)$. This vector contains N complex values that describe the amplitude and phase relations of all antenna elements in the array when a plane wave is incident from an angle θ. With $A_0 = 1$, the definition of the steering vector for the 4-BMAA is given by

$$\boldsymbol{a}(\theta) = (1, \ e^{-j\phi_{\text{out},21}}, \ e^{-j\phi_{\text{out},31}}, \ e^{-j\phi_{\text{out},41}})^{\text{T}} \quad (34)$$

with the phases $\phi_{\text{out},ij}(\theta)$ as defined in (32). The AF can be regarded as the autocorrelation of the antenna steering vector and is defined as follows by [34]:

$$\text{AF}(\theta_i, \theta_j) = \frac{\boldsymbol{a}(\theta_i)^{\text{H}} \cdot \boldsymbol{a}(\theta_j)}{\|\boldsymbol{a}(\theta_i)\| \|\boldsymbol{a}(\theta_j)\|} \quad (35)$$

where $(\cdot)^{\text{H}}$ denotes the Hermitian operator and $\|\cdot\|$ denotes the Euclidean norm of a vector. Usually, only the absolute value of the AF is considered where 0 means perfect orthogonality and 1 means colinearity of the steering vector with itself for the angles θ_i and θ_j. For a nonambiguous angle estimation, a small value of the AF off the main diagonal is therefore desired. The threshold between "ambiguous" and "nonambiguous" is set to 0.5 in this work.

Fig. 13 shows the AF for the conventional ULA [see Fig. 13(a)] and the 4-BMAA [see Fig. 13(b)]. Due to the antenna spacing of $\lambda/2$, no ambiguities are observed besides the main diagonal for the ULA. The AF of the 4-BMAA, however, shows distinct indentions at 0° and 25°, i.e., the beamwidth is supposed to be smaller (21.2° versus 26.2° at $\theta = 0°$). The position of the indentions corresponds to the angular regions where the phase progression of one antenna pair is steepest [see Fig. 12(a)]. The tradeoff of the smaller lobe is an increase in sidelobe level, which limits the ambiguity-free region of the BMAA compared to the ULA ($\pm 38.9°$ versus $\pm 57.8°$).

D. Physical Realization of the Coupling Network

After choosing the desired behavior of the 4-BMAA in terms of phase gain or maximum allowed loss of output power by the modal analysis presented in the previous sections, a set of parameters (G_{C} and B_{C}) is yielded for every individual BMC. The physical realization of an associated BMC based on these parameters is addressed in this section for the exemplary use case at 76.5 GHz. The corresponding antennas and the substrate layer stack-up are already described in Section IV-A.

Every BMC is now regarded as a reciprocal two-port characterized by its scattering parameters. The losses and phase shifts introduced by the two-port are intended to represent the desired attenuation of G_{C} and the phase shifts of B_{C} and the ideal transformer with $\gamma = -1$. For the realization of the 4-BMAA considered in Section IV-C, the transmission
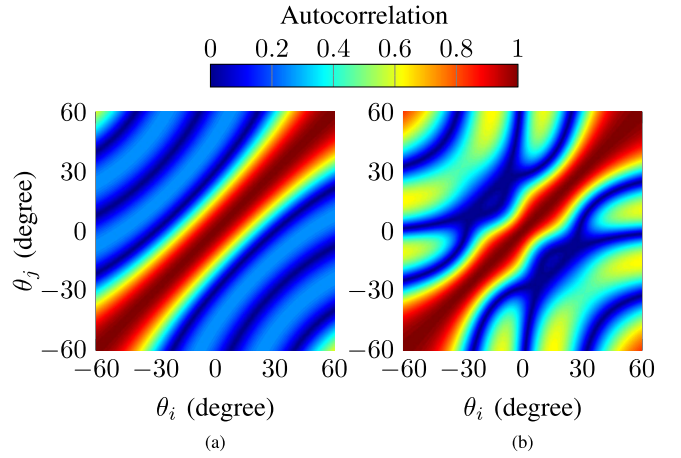

Fig. 13.   Absolute value of the AFs (simulated) of (a) conventional ULA and (b) 4-BMAA using the same antenna elements with identical spacing.
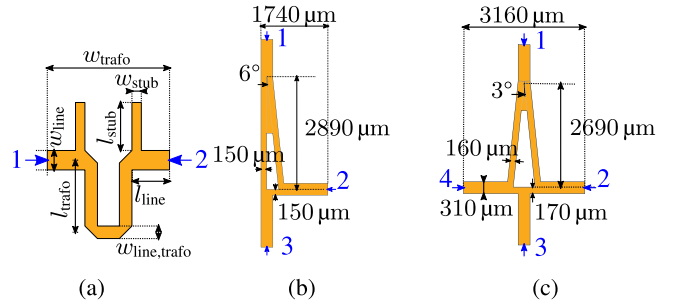

Fig. 14.   Microstrip line components in order to build up the BMC network. (a) Transformer. (b) Two-way power divider. (c) Three-way power divider.

of the BMC should show a phase shift of odd multiples of 180° (in order to represent the turning ratio of $\gamma = -1$ and $B_{\text{C}} = 0$ S) and a loss equal to a series resistance with two times $Z_{\text{C}} = 13\,\Omega$.

In this work, the BMC network is designed as a planar folded microstrip line with two open-ended stubs at its connections points placed on the bottom layer [see Fig. 14(a)]. Its transmission characteristics were optimized by full-wave simulations in order to meet the desired scattering parameter specifications. The main optimization parameters are the length l_{trafo} of the transformer line, the width $w_{\text{line,trafo}}$ of the line, and the spacing between the folded lines. In addition, the stub length l_{stub} and width w_{stub} can be optimized. Following the requirements, the optimized dimensions of the microstrip line transformer of Fig. 14(a) are $w_{\text{trafo}} = 1950\,\mu\text{m}$, $l_{\text{trafo}} = 1290\,\mu\text{m}$, $l_{\text{line,trafo}} = 200\,\mu\text{m}$ $l_{\text{line}} = 700\,\mu\text{m}$, $l_{\text{stub}} = 810\,\mu\text{m}$, and $w_{\text{stub}} = 150\,\mu\text{m}$.

At mm-wave frequencies, however, the microstrip line transformers cannot be simply connected with the antenna feeding lines as additional reflections and transmission losses occur at the microstrip tees. Especially, the tees introduce additional phase shifts that alter the desired phase shift of the BMC. Therefore, a design of three- and four-ports has to be found ensuring the proper phase relations between the antennas. In this work, the tees were replaced by microstrip line couplers designed on the basis of [35] [see Fig. 14(b) and (c)].
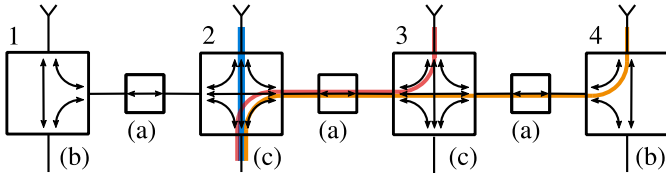
Fig. 15. Composition of the BMC network by means of three transformers and two three- and two-way power dividers each. The block indices (a)–(c) refer to Fig. 14.

TABLE III

SIMULATED S-PARAMETERS OF THE TWO-WAY POWER DIVIDER OF FIG. 14(b) (LEFT) AND THE THREE-WAY POWER DIVIDER OF FIG. 14(c) (RIGHT). THE DIVIDERS ARE SYMMETRICAL, I.E., $s_{21}=s_{41}$ AND $s_{32}=s_{34}$,

$|s_{21}|$	$|s_{31}|$	$|s_{32}|$	$|s_{21}|$	$|s_{31}|$	$|s_{32}|$	$|s_{42}|$
$-4.3\,\mathrm{dB}$	$-2.9\,\mathrm{dB}$	$-4.5\,\mathrm{dB}$	$-6.5\,\mathrm{dB}$	$-4.7\,\mathrm{dB}$	$-6.8\,\mathrm{dB}$	$-8.7\,\mathrm{dB}$

$\angle s_{21}$	$\angle s_{31}$	$\angle s_{32}$	$\angle s_{21}$	$\angle s_{31}$	$\angle s_{32}$	$\angle s_{42}$
$-16°$	$65°$	$81°$	$2°$	$-34°$	$-40°$	$-9°$

In order to derive the required phase relations, the arrangement in Fig. 15 is considered. The phase difference between the red path from antenna 3 to output 2 and the blue path from antenna 2 to output 2 in Fig. 15 is supposed to show the phase shift of the BMC, in this work $-180°$. This phase shift is already realized using the microstrip transformer. Therefore, the remaining phase contributions of the power dividers need to cancel each other, i.e.,

$$\angle s_{41} + \angle s_{32} - \angle s_{31} = n \cdot 360°, \quad n \in \mathbb{Z} \tag{36}$$

with indices referring to Fig. 14(c). In order to account for the coupling of antennas through more than one BMC, the phases of the orange path from antenna 4 to output 2 and the blue path shall differ two times the phase shift of one microstrip transformer, in this work $-360°$. Considering (36), it follows:

$$\angle s_{42} = n \cdot 360°, \quad n \in \mathbb{Z}. \tag{37}$$

Based on the requirements in (36) and (37), the power dividers were designed using full-wave simulations. Its dimensions are given in Fig. 14 and the simulated transmission S-parameters are shown in Table III.

The additional losses of the power dividers, however, lead to a decrease in the phase gain of the 4-BMAA. The final design, therefore, shows a slightly different characteristic than intended in the design. Based on the full-wave simulations of the whole structure, the realized design reflects a coupling impedance of $Z_C = Z_{C2} = 17\,\Omega \parallel 40\,\mathrm{fF}$, and therefore, a smaller phase gain is expected. The additional imaginary component in Z_C results from the fact that (36) and (37) are not perfectly satisfied. The layout of the designed BMC is shown in Fig. 16.

The width of the coupling network in the presented form exceeds the spacing of the antenna elements of 1.95 mm. This may be prevented by a codesign of transformer and power divider. However, in order to quickly exchange the BMC in future designs, the presented solution is more straightforward. In order to adapt the designed BMC to the antennas, the circuit components were bent at the arrows in Fig. 16. The different lengths of the lines connecting the antennas to
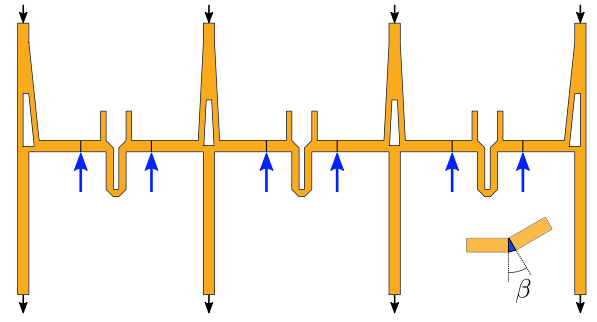

Fig. 16. Layout of the 4-BMAA coupling network with three transformers and four couplers. The blue arrows mark the points where the lines are bent by an angle of $\beta = 10°$ in order to adjust to an antenna spacing of $d = \lambda/2$.
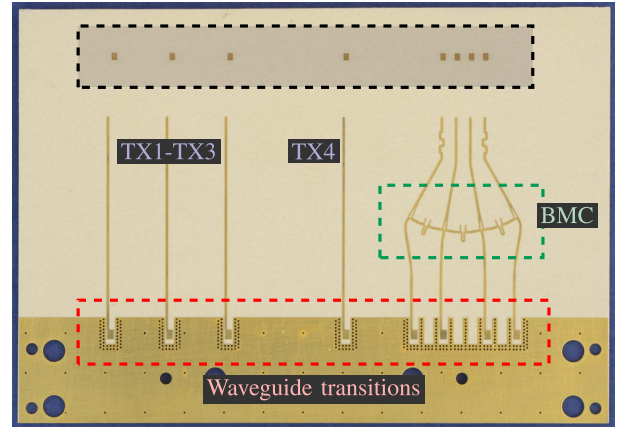

Fig. 17. Back view of the realized 4-BMAA. The inset (black dashed line) shows the patch antennas on the top layer. The overall PCB size is 80 mm × 56 mm.

the BMC were compensated by meander lines between the outer antenna elements and the BMC. This ensures a uniform phase distribution at all inputs of the BMC for a vertically incident wave. A photograph of the fabricated antenna PCB is shown in Fig. 17.

E. Measurements

This section presents the measurement setup and the measurement results of the fabricated 4-BMAA. In order to measure the multichannel antenna array in a convenient way, radar measurements in the frequency range from 75.5 to 76.5 GHz with a multichannel radar with interchangeable antenna front end were conducted. The radar was placed on a turntable in an anechoic chamber, and a corner reflector with a radar cross section (RCS) of 8.5 dBsm was placed as a target in a distance of 4.4 m under an angle $\theta = 0°$ to the radar. In order to characterize the θ-dependence of the 4-BMAA, the turntable was rotated in the angular range of $\theta = -60\ldots+60°$. The setup and the radar system are shown in Fig. 18. The 4-BMAA on the PCB acts as the receive antenna array, whereas four additional antennas (TX1–TX4) are placed on the PCB, which acts as transmitting antennas. However, in the measurements, only the outer transmit antenna (i.e., TX1 in Fig. 17) was used. For comparison, an equivalent PCB with the same antenna elements at the same positions but without BMC network was also fabricated and measured.
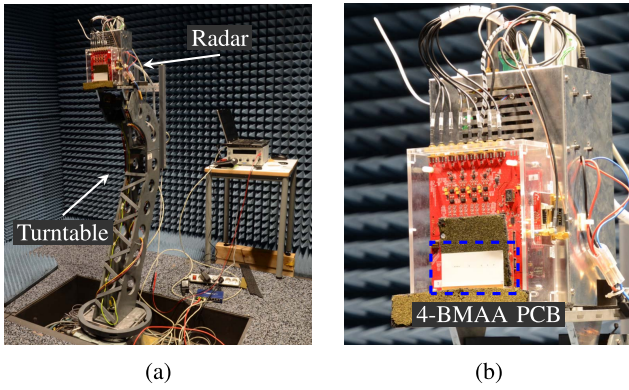
Fig. 18. Measurement setup in the anechoic chamber with (a) radar mounted on a turntable and (b) close-up view of the 77 GHz radar with the 4-BMAA PCB of Fig. 16 applied.
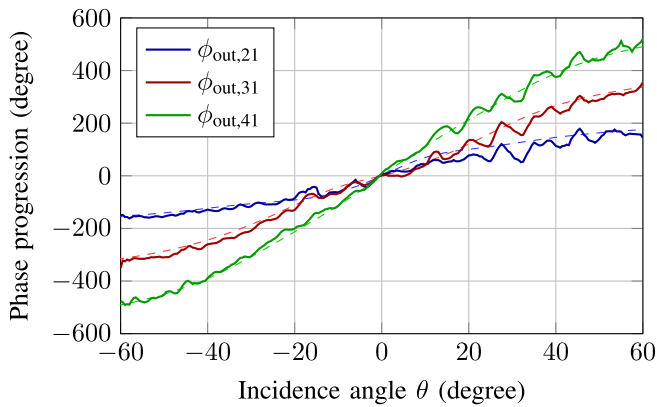

Fig. 19. Measured (———) and theoretical (– – –) (with $Z_C = Z_{C2} = 17\,\Omega \parallel 40\,\text{fF}$) phase progression of the fabricated 4-BMAA with respect to the first antenna element in the array.

The measured radar signals for every angle θ and every receiving channel were processed using a range-Doppler processing [36], i.e., a 2-D FFT. Afterward, the amplitude and phase of the range-Doppler matrix were extracted at the target position in order to calculate the phase progression.

Fig. 19 shows the measured phase progression normalized to the first antenna in the array in comparison to the theoretical values with $Z_C = Z_{C2} = 17\,\Omega \parallel 40\,\text{fF}$ calculated by the modal analysis in Section IV. The respective AFs are shown in Fig. 20. A very good match between theory and measurements can be observed with peak phase gains $\eta_{21} \approx 2.4$ at boresight and $\eta_{31} \approx 1.4$ at $\theta = \pm 27°$, respectively. The measurements show some ripples for positive values of θ which are due to perturbations in the measurement setup and lead to a disturbed AF for positive angles.

The indentions in the main diagonal and the associated narrower main lobe, which were already addressed in the discussions regarding Fig. 13(b), are clearly visible but are less pronounced here due to the losses of the real system. This confirms the correctness of the underlying theory regarding multichannel BMAAs. The 3 dB beamwidth around the boresight direction is reduced from 26.2° of the conventional array [Fig. 13(a)] to 23.2° for the 4-BMAA. For the second indention at $\theta = -27°$, the beamwidth is reduced by 5.1° from 29.9° for the conventional array to 24.8° for the BMAA.
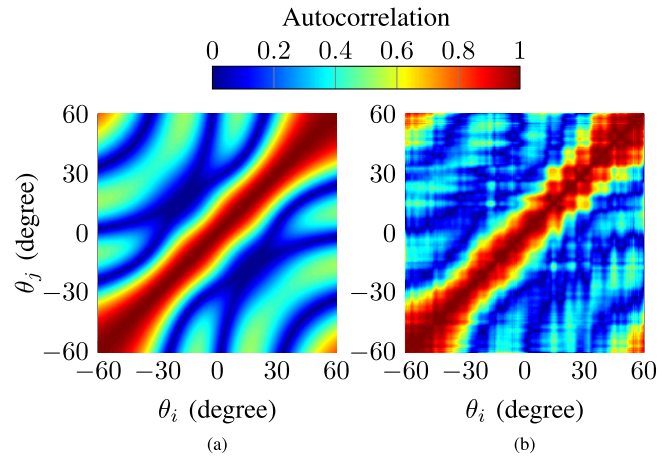

Fig. 20. Absolute value of the AF of the fabricated 4-BMAA with $Z_C = Z_{C2} = 17\,\Omega \parallel 40\,\text{fF}$. (a) Theoretical. (b) Measured.
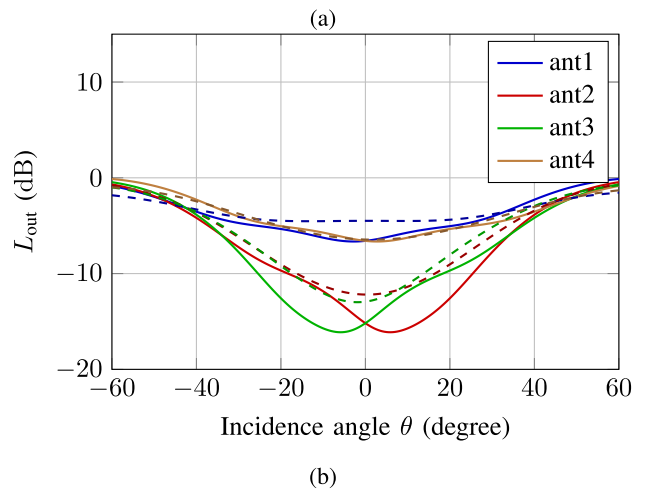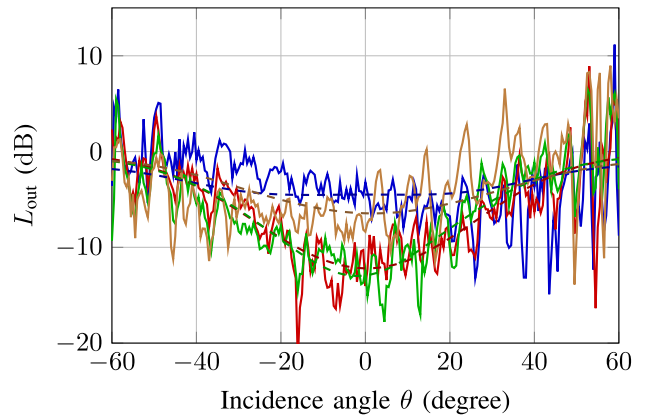

Fig. 21. (a) Measured curves of the fabricated 4-BMAA and (b) theoretical curves assuming $Z_C = Z_{C2} = 17\,\Omega \parallel 40\,\text{fF}$ of the normalized output power L_{out}. The dashed lines in both plots are identical and represent a model fit of the measured data.

The measurements of the normalized output power L_{out} for the 4-BMAA are shown in Fig. 21(a) for every individual antenna. The curves are constructed by dividing the amplitudes of the target extracted from the 4-BMAA radar measurement and the target extracted from the ULA measurement according to (3). Due to a lot of ripples in the measurement results

because of parasitic influences of the measurement setup, a nonlinear model-based curve fitting was performed (see the dashed lines in Fig. 21). Fig. 21(a) shows that the loss of output power is more pronounced at antennas 2 and 3 than at antennas 1 and 4. This is in accordance with the theory [see Fig. 21(b)], and a good match between the measurements and the theory is observable. For the outer antennas in the array, antennas 1 and 4, the maximum loss is about 4.5 and 6.5 dB, respectively. Antennas 2 and 3 have a minimum normalized output power of about -12.2 and -13.0 dB, respectively, compared to the uncoupled array. The reduction of the output power for these two antennas is, therefore, lower than the theoretical value of about $L_{out} = -16$ dB.

V. CONCLUSION

In this article, a comprehensive, general concept for designing and analyzing BMAAs with an arbitrary but even number of antenna elements has been introduced. The conventional theory on two-element BMAAs has been generalized both on the circuit level and with respect to the modal analysis. The effects of applying varying levels of BMC to an antenna array have been highlighted. The presented methodology was applied in order to design a BMAA with four antenna elements at 76.5 GHz. Radar measurements with the fabricated prototype verified the theoretical findings.

REFERENCES

[1] J. Hasch, E. Topak, R. Schnabel, T. Zwick, R. Weigel, and C. Waldschmidt, "Millimeter-wave technology for automotive radar sensors in the 77 GHz frequency band," *IEEE Trans. Microw. Theory Techn.*, vol. 60, no. 3, pp. 845–860, Mar. 2012.

[2] J. Lien *et al.*, "Soli: Ubiquitous gesture sensing with millimeter wave radar," *ACM Trans. Graph.*, vol. 35, no. 4, pp. 1–19, 2016.

[3] Z. Peng, L. Ran, and C. Li, "A *K*-band portable FMCW radar with beamforming array for short-range localization and vital-Doppler targets discrimination," *IEEE Trans. Microw. Theory Techn.*, vol. 65, no. 9, pp. 3443–3452, Sep. 2017.

[4] P. Hugler, F. Roos, M. Schartel, M. Geiger, and C. Waldschmidt, "Radar taking off: New capabilities for UAVs," *IEEE Microw. Mag.*, vol. 19, no. 7, pp. 43–53, Nov. 2018.

[5] C. A. Balanis, *Antenna Theory: Analysis and Design*, 3rd ed. Hoboken, NJ, USA: Wiley, 2005.

[6] F. C. Robey, S. Coutts, D. Weikle, J. C. McHarg, and K. Cuomo, "MIMO radar theory and experimental results," in *Proc. Conf. Rec. 38th Asilomar Conf. Signals, Syst. Comput.*, Pacific Grove, CA, USA, Nov. 2004, pp. 300–304.

[7] J. Li and P. Stoica, *MIMO Radar Signal Processing*, 1st ed. Hoboken, NJ, USA: Wiley, 2008.

[8] A. Chadwick, "Superresolution for high-frequency radar," *IET Radar, Sonar Navigat.*, vol. 1, no. 6, p. 431, 2007.

[9] C. Fischer, H.-L. Bloecher, W. Menzel, J. Dickmann, and F. Ruf, "Evaluation of different super-resolution techniques for automotive applications," in *Proc. IET Int. Conf. Radar Syst. (Radar)*, Glasgow, U.K., Oct. 2012, pp. 1–6.

[10] R. N. Miles, D. Robert, and R. R. Hoy, "Mechanically coupled ears for directional hearing in the parasitoid fly ormia ochracea," *J. Acoust. Soc. Amer.*, vol. 98, no. 6, pp. 3059–3070, Dec. 1995.

[11] A. R. Masoumi, Y. Yusuf, and N. Behdad, "Biomimetic antenna arrays based on the directional hearing mechanism of the parasitoid fly ormia ochracea," *IEEE Trans. Antennas Propag.*, vol. 61, no. 5, pp. 2500–2510, May 2013.

[12] W. Cade, "Acoustically orienting parasitoids: Fly phonotaxis to cricket song," *Science*, vol. 190, no. 4221, pp. 1312–1313, Dec. 1975. [Online]. Available: https://science.sciencemag.org/content/190/4221/1312

[13] A. C. Mason, M. L. Oshinsky, and R. R. Hoy, "Hyperacute directional hearing in a microscale auditory system," *Nature*, vol. 410, no. 6829, pp. 686–690, Apr. 2001. [Online]. Available: http://www.nature.com/nature/journal/v410/n6829/full/410686a0.html

[14] A. R. Masoumi and N. Behdad, "An improved architecture for two-element biomimetic antenna arrays," *IEEE Trans. Antennas Propag.*, vol. 61, no. 12, pp. 6224–6228, Dec. 2013.

[15] P. Gruner, T. Chaloun, and C. Waldschmidt, "A generalized model for two-element biomimetic antenna arrays," *IEEE Trans. Antennas Propag.*, vol. 67, no. 3, pp. 1630–1639, Mar. 2019.

[16] M. Akçakaya and A. Nehorai, "Biologically inspired coupled antenna beampattern design," *Bioinspiration Biomimetics*, vol. 5, no. 4, Dec. 2010, Art. no. 046003. [Online]. Available: http://iopscience.iop.org/1748-3190/5/4/046003

[17] Y. Zang, H. Luyen, H. R. Bahrami, and N. Behdad, "An analytic synthesis method for two-element biomimetic antenna arrays," *IEEE Trans. Antennas Propag.*, vol. 68, no. 4, pp. 2797–2809, Apr. 2020.

[18] J. Zhong, A. Kiourti, and J. L. Volakis, "Reducing and controlling the beamwidth of electrically small antenna arrays," in *Proc. 9th Eur. Conf. Antennas Propag. (EuCAP)*, Lisbon, Portugal, Apr. 2015, pp. 1–2.

[19] A. M. Elfrgani and R. G. Rojas, "Biomimetic antenna array using non-foster network to enhance directional sensitivity over broad frequency band," *IEEE Trans. Antennas Propag.*, vol. 64, no. 10, pp. 4297–4305, Oct. 2016.

[20] P. Gruner, T. Chaloun, and C. Waldschmidt, "Towards a mm-wave planar biomimetic antenna array with enhanced phase sensitivity," in *Proc. 10th Eur. Conf. Antennas Propag. (EuCAP)*, Apr. 2016, pp. 1–5.

[21] P. Grüner, D. Schmucker, and C. Waldschmidt, "A new coupling network topology for mm-wave biomimetic antenna arrays," in *Proc. 13th German Microw. Conf. (GeMiC)*, Cottbus, Germany, Mar. 2020, pp. 32–35.

[22] F. T. Dagefu, J. Oh, and K. Sarabandi, "A sub-wavelength RF source tracking system for GPS-denied environments," *IEEE Trans. Antennas Propag.*, vol. 61, no. 4, pp. 2252–2262, Apr. 2013.

[23] P. Gruner, M. Geiger, and C. Waldschmidt, "Ultracompact monostatic MIMO radar with nonredundant aperture," *IEEE Trans. Microw. Theory Techn.*, vol. 68, no. 11, pp. 4805–4813, Nov. 2020.

[24] P. Gruner, T. Chaloun, and C. Waldschmidt, "Enhanced angle estimation accuracy of ultra compact radars inspired by a biomimetic approach," in *IEEE MTT-S Int. Microw. Symp. Dig.*, Honolulu, HI, USA, Jun. 2017, pp. 1425–1428.

[25] R. J. Kozick, F. T. Dagefu, and B. M. Sadler, "Two-element biomimetic antenna array design for power extraction / phase amplification tradeoff," in *Proc. 14th Eur. Conf. Antennas Propag. (EuCAP)*, Copenhagen, Denmark, Mar. 2020.

[26] R. J. Kozick, F. T. Dagefu, and B. M. Sadler, "Two-element biomimetic antenna array design and performance," in *Proc. IEEE Int. Conf. Acoust., Speech Signal Process. (ICASSP)*, May 2020, pp. 4747–4751.

[27] A. R. Masoumi and N. Behdad, "Architecture, design, and non-linear optimization of three-element biomimetic antenna arrays," *IEEE Antennas Wireless Propag. Lett.*, vol. 12, pp. 1416–1419, Nov. 2013.

[28] M. Ranjbar Nikkhah, K. Ghaemi, and N. Behdad, "A three-element biomimetic antenna array with an electrically small triangular lattice," *IEEE Trans. Antennas Propag.*, vol. 65, no. 8, pp. 4007–4016, Aug. 2017.

[29] M. Akcakaya, C. H. Muravchik, and A. Nehorai, "Biologically inspired coupled antenna array for direction of arrival estimation," in *Proc. Conf. Rec. Forty 4th Asilomar Conf. Signals, Syst. Comput.*, Pacific Grove, CA, USA, Nov. 2010, pp. 1961–1965.

[30] D. M. Pozar, *Microwave Engineering*, 3rd ed. Hoboken, NJ, USA: Wiley, 2005.

[31] J. C. Mason and D. C. Handscomb, *Chebyshev Polynomials*, 1st ed. Boca Raton, FL, USA: CRC Press, Sep. 2002.

[32] I. N. Bronštejn, K. A. Semendjaev, G. Musiol, and H. Mühlig, *Handbook of Mathematics*, 6th ed. Berlin, Germany: Springer, 2015.

[33] C. Alexander, *Fundamentals of Electric Circuits*, 5th ed. New York, NY, USA: McGraw-Hill, 2013.

[34] M. Eric, A. Zejak, and M. Obradovic, "Ambiguity characterization of arbitrary antenna array: Type I ambiguity," in *Proc. IEEE 5th Int. Symp. Spread Spectr. Techn. Appl. Spread Technol. Afr.*, vol. 2. Sun City, South Africa, Sep. 1998, pp. 399–403.

[35] G.-Y. Chen, J.-S. Sun, and S.-Y. Huang, "The novel 3-Way power Dividers/Combiners structure and design," in *Proc. IEEE Annu. Wireless Microw. Technol. Conf.*, Clearwater Beach, FL, USA, Dec. 2006, pp. 1–4.

[36] V. Winkler, "Range Doppler detection for automotive FMCW radars," in *Proc. Eur. Microw. Conf.*, Munich, Germany, 2007, pp. 166–169.

Patrik Grüner (Member, IEEE) received the M.Sc. degree in electrical engineering from Ulm University, Ulm, Germany, in 2015, where he is currently pursuing the Ph.D. degree.

In 2015, he joined the Institute of Microwave Engineering (MWT), Ulm University. His current research interests include compact frequency-modulated continuous wave (FMCW) radar sensors and biomimetic antenna systems both in the microwave and millimeter-wave range.

Mr. Grüner was a recipient of the ARGUS Science Award in 2013 and the Best Paper Award of the 2013 International Workshop on Antenna Technology.

Ines Dorsch received the M.Sc. degree in electrical engineering from Ulm University, Ulm, Germany, in 2019, where she is currently pursuing the Ph.D. degree with the Institute of Microwave Engineering.

Her current research interests include biomimetic antenna systems in the microwave and millimeter-wave range and their application in sensor networks.

Mr. Dorsch was a recipient of the ARGUS Science Award in 2019.

Christian Waldschmidt (Senior Member, IEEE) received the Dipl.Ing. (M.S.E.E.) and Dr.Ing. (Ph.D.E.E.) degrees from the University of Karlsruhe (TH), Karlsruhe, Germany, in 2001 and 2004, respectively.

From 2001 to 2004, he was a Research Assistant with the Institut für Höchstfrequenztechnik and Elektronik (IHE), TH. Since 2004, he has been with Robert Bosch GmbH, Stuttgart, Germany, in the business units Corporate Research and Chassis Systems. He was heading different research and development teams in microwave engineering, RF sensing, and automotive radar. In 2013, he returned to academia. He was appointed as the Director of the Institute of Microwave Engineering, Ulm University, Ulm, Germany, as a Full Professor. He has authored or coauthored over 200 scientific publications and more than 20 patents. The research topics focus on radar and RF sensing, millimeter-wave and submillimeter-wave engineering, antennas and antenna arrays, and RF and array signal processing.

Dr. Waldschmidt is a member of the Executive Committee Board of the German MTT/AP Joint Chapter and the German Information Technology Society (ITG). He was a co-recipient of 11 best paper awards. He served as the Chair for the IEEE MTT-27 Technical Committee on wireless-enabled automotive and vehicular applications. He was the two-time TPC Chair and the General Chair of the IEEE MTT International Conference on Microwaves for Intelligent Mobility. Since 2018, he has been serving as an Associate Editor for IEEE MTT MICROWAVE WIRELESS COMPONENTS LETTERS (MWCL). He is a reviewer for multiple IEEE TRANSACTIONS and many IEEE conferences in the field of microwaves.